



# Finite Element Prediction of the Thermal Conductivity of GNP/Al Composites

X. S. Yang<sup>1</sup> · L. Zhou<sup>1</sup> · K. Y. Liu<sup>1</sup> · Z. Y. Liu<sup>2</sup> · Q. Z. Wang<sup>2</sup> · B. L. Xiao<sup>2</sup> · Z. Y. Ma<sup>2</sup>

Received: 7 April 2021 / Revised: 9 June 2021 / Accepted: 27 June 2021 / Published online: 20 August 2021  
© The Chinese Society for Metals (CSM) and Springer-Verlag GmbH Germany, part of Springer Nature 2021

## Abstract

A 3D multi-scale finite element model was developed to predict the effective thermal conductivity of graphene nanoplatelet (GNP)/Al composites. The factors influencing the effective thermal conductivity of the GNP/Al composites were investigated, including the orientation, shape, aspect ratio, configuration and volume fraction of GNPs. The results show that GNPs shape has a little influence on the thermal conductivity of GNP/Al composites, and composites with elliptic GNPs have the highest thermal conductivity. In addition, with increasing the aspect ratio of GNPs, the thermal conductivity of GNP/Al composites increases and finally tends to be stable. The GNPs configuration strongly influences the thermal conductivity of GNP/Al composites, and the thermal conductivity of the composites with layered GNPs is the highest among the five configurations. The effective thermal conductivity is sensitive to volume fraction of GNPs. Ideally, when the volume fraction of layered GNPs reaches 1.54%, the thermal conductivity of GNP/Al composites is as high as 400 W/m K. The findings of this study could provide a good theoretical basis for designing high thermal conductivity GNP/Al composites.

**Keywords** Multi-scale finite element model · Thermal conductivity · GNP/Al composites · Shape · Aspect ratio · Configuration

## 1 Introduction

Nanocarbon materials are considered as an ideal filler due to the peculiar properties, such as high modulus, extremely high thermal conductivity (3000 W/m K for carbon nanotubes [1] and 5300 W/m K for single layer graphene [2]) and light weight. Also, (graphene nanoplatelets) GNPs can be derived from the plentiful resource of natural graphite conveniently and cost-effectively [3] and have been used as nano-reinforcement in Al matrix composites [4, 5]. Hence, GNP/Al composites with high thermal conductivity and

low thermal expansion are in strong demand for solving the heat dissipation problem caused by miniaturization [6]. It is expected that in future, GNP/Al composites will be widely used in the field of microelectronics, such as electronics, batteries, aerospace devices and LED lightings. [7, 8].

In recent years, the fabrication method, microstructure and mechanical properties of GNP/Al composites have been extensively investigated [9–12]. The strengthening mechanism of GNP/Al composites was discussed based on the load transfer strengthening, Orowan strengthening and dislocations strengthening. Results showed that the fabricating procedure, dispersion and content of GNPs, as well as interfacial microstructure, affect the mechanical properties of GNP/Al composites significantly. In addition to mechanical properties, the high thermal conductivity of GNP/Al composites is also very important. However, relatively little consideration has been given to the thermal conductivity of GNP/Al composites so far.

Chi-Hoon et al. [13] studied the thermal conductivity of GNP/Al composites fabricated by friction stir processing. They reported that the thermal conductivity of the GNP/Al composites was increased by more than 15% in comparison with that of the aluminum matrix. Abdollah et al. [14] investigated the microstructure and thermal conductivity of GNP/Al

Available online at <http://link.springer.com/journal/40195>.

✉ L. Zhou  
lizhou@ytu.edu.cn

✉ B. L. Xiao  
blxiao@imr.ac.cn

<sup>1</sup> School of Electromechanical and Automotive Engineering, Yantai University, Yantai 264005, China

<sup>2</sup> Shi-Changxu Innovation Center for Advanced Materials, Institute of Metal Research, Chinese Academy of Sciences, Shenyang 110016, China

composites fabricated by powder metallurgy and hot rolling techniques. The uniform dispersion of GNPs at low content and agglomeration at higher content was confirmed. Accordingly, the thermal conductivity of composites was improved at low GNP content and decreased at high GNP content.

Furthermore, the multi-phase GNP + B<sub>4</sub>C/Al-Si hybrid composites were produced by semi-powder and pressure infiltration methods [15]. Results showed that thermal conductivity decreased with increasing B<sub>4</sub>C content, but increased with the increase in graphene content, and the best experimental result was a 16% increase with 0.5 vol.% GNPs. Wang et al. [16] fabricated the vertically aligned GNPs on the surfaces of graphite (Gr) flakes and prepared the Gr (GNP)/Al composites with different GNPs contents. It was observed that the through-plane thermal conductivity of Gr (GNP)/Al composites can be improved by 96.8% with GNPs content increasing up to 3.3 vol.%. Evans et al. [17] predicted the effective thermal conductivity of nanocomposites by using three-level homogenization theory, and concluded that thermal conductivity might be significantly enhanced as a result of particles aggregation.

The existing investigations show that both the dispersion state and the orientation arrangement of GNPs affect the performance of GNP/Al composites significantly. However, the relationship between microstructure and thermal properties has not been fully understood yet. With the increasing requirement of GNP/Al composites, a fast design method to predict the thermal properties of new GNP/Al composites is in demand. Finite element simulation is an important method to deeply understand the thermal conductivity of GNP/Al composites to optimize the microstructural design.

In the past, although there are many simulative studies on the effects of content, agglomeration degree and arrangement of GNPs on the thermal conductivity of GNP/polymer composites [18–20], there are few simulations on the thermal properties of GNP/Al composites. Therefore, the application of the finite element method (FEM) to investigate the quantitative relationship between the thermal conductivity and the microstructures of GNP/Al composites is essential.

In this study, a three-dimensional multi-scale model was developed using FEM to evaluate the thermal behavior of GNP/Al composites based on continuum mechanics. The effects of shape, aspect ratio, configuration and volume fraction of GNPs on the thermal conductivity were investigated.

## 2 Finite Element Modeling

### 2.1 3D Model and Material Properties

Generally, single layer GNP offers a higher thermal conductivity than that of multiple layers GNP, and the thermal conductivity of GNPs ranges from 3000 to 5000 W/m K depending

on the defect concentration and roughness of the edges [2]. In this study, considering the strong tendency of the graphene to stick together, the GNPs were represented by multiple layers graphene instead of a single layer. To simplify the model, the interfacial thermal barrier resistance between GNPs and the matrix is assumed to be included in the deduced thermal conductivity value of GNPs. Rule of mixtures (ROM) equation is widely used to predict the basic properties of materials, such as density, modulus and thermal conductivity. So, considering the interface layer and the anisotropic of GNPs thermal conductivity along the in-plane and cross-plane directions [21], the thermal conductivity of GNPs  $\lambda_{\parallel(\perp)}$  can be expressed as [22]:

$$\lambda_{\parallel(\perp)} = \lambda_{\parallel(\perp)0}(V_G) + \lambda_I(V_I), \quad (1)$$

where  $V_I$  and  $V_G$  are the volume fractions of interface and GNPs,  $\lambda_{\parallel(\perp)0}$  are thermal conductivities of GNPs itself,  $\lambda_I$  is the thermal conductivities of interface. Here, the thermal conductivities of GNPs in-plane and cross-plane are  $\lambda_{\parallel 0} = 3478 \text{ W/mK}$  and  $\lambda_{\perp 0} = 19 \text{ W/m K}$  [23], respectively. The thermal conductivity of interface (Al<sub>4</sub>C<sub>3</sub>) is  $\lambda_I = 140 \text{ W/m K}$  [24]. Therefore, the three-phase material can be represented by the two-phase model, as shown in Fig. 1. The interphase is assumed to lie on both sides of the GNPs, and the average interfacial thickness of GNP is set as  $t_I = 0.34 \text{ nm}$ . The average thickness of multi-layered GNPs is expressed as  $t_G = n * t_s$  ( $n$  is the average layer number of GNPs, and  $t_s$  is the thickness of single-layered GNP). Moreover, the interface between the GNPs and Al matrix was considered perfectly bonded.

In this work, the finite element software ABAQUS was used to establish a representative volume element (RVE) model of GNP/Al composites. As shown in Fig. 2, the model is divided into two parts: aluminum matrix and GNPs. The cubic cell represents matrix, and rectangular sheets represent GNPs [25–27]. The Boolean operation in Abaqus/CAE was used to cut the matrix with GNPs, and then, GNPs were embedded into the matrix to obtain a complete RVE model, as shown in Fig. 2b. Generally, the thickness of multiple layers GNPs is in the range from about 2–10 nm, with the

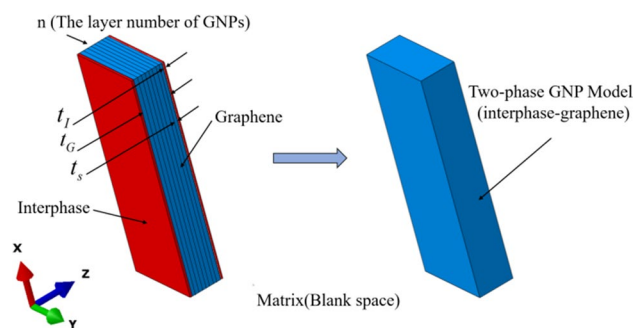
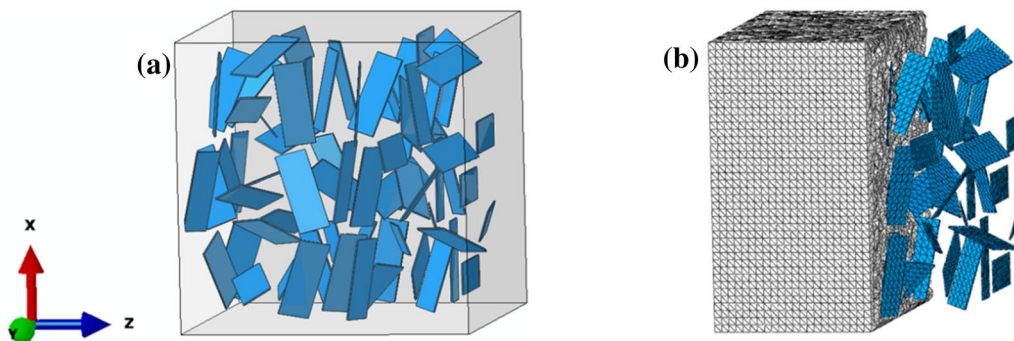


Fig. 1 Simplifying the model by combining the interface with GNPs



**Fig. 2** A three-dimensional randomly distributed GNP/Al composites model, **a** the geometrical model of RVE and **b** the nodes on the GNPs embedded in matrix

**Table 1** Material properties entered in ABAQUS [29–31]

Properties	Aluminum	GNPs
Thermal conductivity (W/m K)		
In-plane	217	3000
Cross-plane	217	36
Density ( $10^{-9}$ ton/mm <sup>3</sup> )	2.7	1.5
Specific heat ( $10^8$ mJ/ton K)	8.8	7.1

number of GNP layers of 10 or so [28]. Hence, we take the GNPs thickness of 5 nm ( $t_G$ ) to calculate the thermal conductivity. By calculating, the in-plane and cross-plane thermal conductivities of GNPs are 3000 W/m K and 36 W/m K, respectively. The material properties of aluminum and GNPs entered in the software are listed in Table 1 [29–31]. The size of cubic cell is  $1 \mu\text{m} \times 1 \mu\text{m} \times 1 \mu\text{m}$ , and the size of GNP is  $280 \text{ nm} \times 110 \text{ nm} \times 5 \text{ nm}$ .

### 2.2 Meshing

Due to the irregularity of geometric model, 10-noded quadratic tetrahedron heat transfer elements (DC3D10) in ABAQUS were used to mesh. It is well known that the size of the element affects the calculation accuracy and calculation time. Figure 3 shows the variation of the average heat flux and the calculation time with the size of element. From the figure, it can be seen that the average heat flux of GNP/Al composites and computation time increase with decreasing the element size, and when the elements size is about 10 nm, the average heat flow density growth tends to be stable. Considering the accuracy and analysis efficiency, the element size is selected as 10 nm.

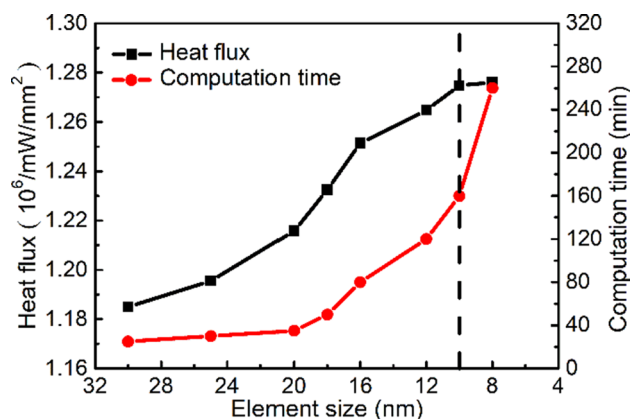


**Fig. 3** Variation of average heat flux and computation time with element size

### 2.3 Temperature Load and Heat Transfer Direction

For the three-dimensional steady-state thermal analysis, the heat exchange caused by convection and radiation is not considered, and only the heat conduction is considered. As shown in Fig. 4a, the temperature gradient is along the  $x$  direction. Specifically, the top and bottom surfaces of the model are maintained at temperatures of 26 and 24 °C, and the other surfaces keeping adiabatic; thus, this allows the heat to flow in negative  $x$  direction only. According to Fourier's law [32], the relationship between the average heat flux and the thermal conductivity is as follows:

$$\lambda = q^{\text{avg}} \times \frac{\Delta L}{\Delta T} \tag{2}$$

where  $\lambda$  is the effective thermal conductivity,  $q^{\text{avg}}$  is the average heat flux of GNP/Al composites,  $\Delta T$  is the temperature difference between upper and lower surfaces in the  $x$  direction, and  $\Delta L$  is the distance between the high and low temperature surfaces of the model.

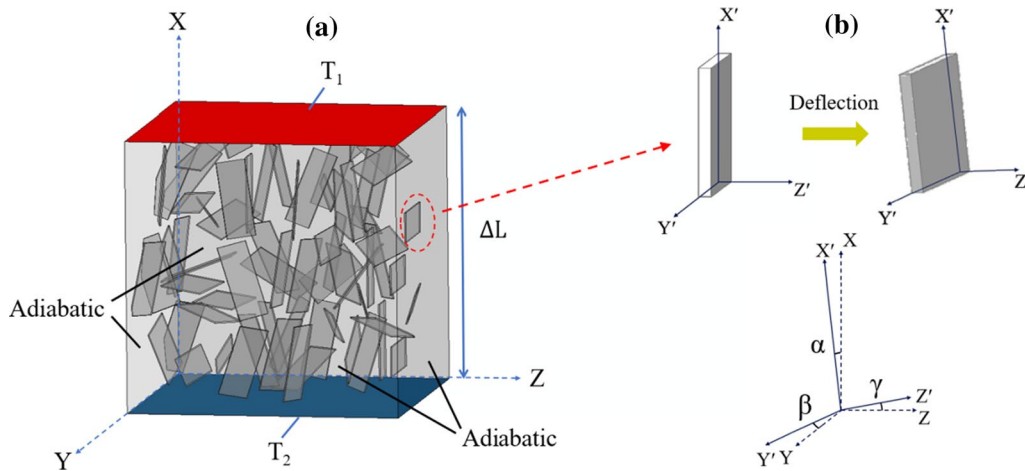


**Fig. 4** Simplified diagrams of GNP/Al composites: **a** temperature gradient of RVE along  $x$  direction and **b** local coordinates based on GNP

Therefore, the heat flux of all nodes is determined from the calculation results, and the average heat flux can be obtained by:

$$q^{\text{avg}} = \frac{\sum_{i=1}^n q_i}{n} \quad (3)$$

where  $q_i$  is the heat flux of the node,  $n$  is the number of nodes. Then, the thermal conductivity in the  $x$  direction of GNP/Al composites can be obtained from Eq. (2).

Due to the random distribution of GNPs in the RVE, the effect of positions of GNPs on the thermal conductivity should be considered when investigating the heat transfer process. As shown in Fig. 4b, when GNP is deflected in the matrix, angles between the local coordinates based on the principal axes of GNP,  $X'-Y'-Z'$ , and the global coordinates,  $X-Y-Z$ , were simplified to be three average values,  $\alpha$ ,  $\beta$  and  $\gamma$ , respectively. The relationship between the two coordinate systems is given by [33]:

$$\begin{bmatrix} x \\ y \\ z \end{bmatrix} = C \begin{bmatrix} x' \\ y' \\ z' \end{bmatrix} = C_1 C_2 C_3 \begin{bmatrix} x' \\ y' \\ z' \end{bmatrix} \quad (4a)$$

in which

$$C_1 = \begin{bmatrix} \cos\alpha & -\sin\alpha & 0 \\ \sin\alpha & \cos\alpha & 0 \\ 0 & 0 & 1 \end{bmatrix}, C_2 = \begin{bmatrix} 1 & 0 & 0 \\ 0 & \cos\beta & -\sin\beta \\ 0 & \sin\beta & \cos\beta \end{bmatrix}, C_3 = \begin{bmatrix} \cos\gamma & 0 & -\sin\gamma \\ 0 & 1 & 0 \\ \sin\gamma & 0 & \cos\gamma \end{bmatrix} \quad (4b)$$

$$C = C_1 C_2 C_3 = \begin{bmatrix} \cos\alpha\cos\gamma + \sin\alpha\sin\beta\sin\gamma & -\sin\alpha\cos\beta & -\cos\alpha\sin\gamma + \sin\alpha\sin\beta\cos\gamma \\ \sin\alpha\cos\gamma - \cos\alpha\sin\beta\sin\gamma & \cos\alpha\cos\beta & -\sin\alpha\sin\gamma - \cos\alpha\sin\beta\cos\gamma \\ \cos\beta\sin\gamma & \sin\beta & \cos\beta\cos\gamma \end{bmatrix} \quad (4c)$$

Then, the thermal conductivity conversion relationship of GNPs in global coordinates and local coordinates can be described as:

$$\begin{bmatrix} \lambda_{xx} & \lambda_{xy} & \lambda_{xz} \\ \lambda_{yx} & \lambda_{yy} & \lambda_{yz} \\ \lambda_{zx} & \lambda_{zy} & \lambda_{zz} \end{bmatrix} = C^{-1} \begin{bmatrix} \lambda'_x & 0 & 0 \\ 0 & \lambda'_y & 0 \\ 0 & 0 & \lambda'_z \end{bmatrix} C \quad (5)$$

Therefore, the thermal conductivity of GNPs in global coordinates is affected by their distribution.

## 3 Results and Discussion

### 3.1 Influence of GNPs Shape

In order to investigate the influence of the shape of the GNPs on the thermal conductivity of GNP/Al composites, the RVE models with different GNPs shapes were established, as shown in Fig. 5. The typical shapes of GNPs are ellipse, rectangle, circle, polygon and square, and the volume fraction of GNPs is 0.25%. In order to avoid the change of thermal conductivity caused by the deflection of GNPs

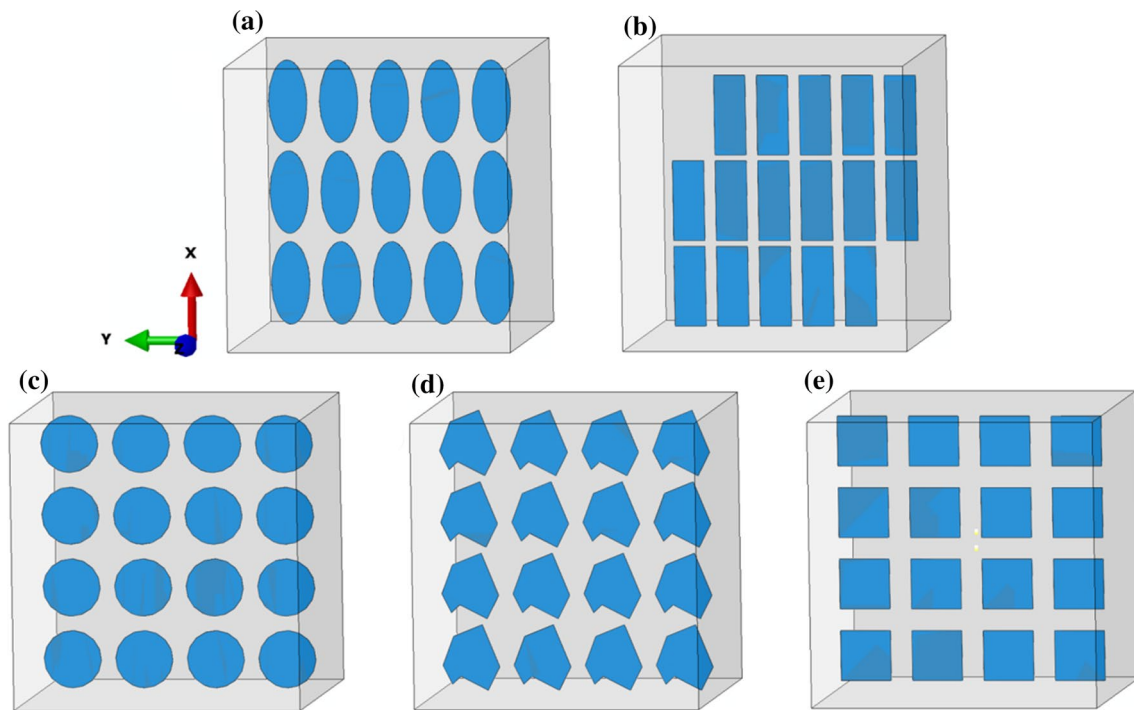


**Fig. 5** Schematics of RVE with different shapes of GNPs: **a** ellipse, **b** rectangle, **c** circle, **d** polygon, **e** square

(described in Sect. 2.3), the arrangement direction of GNPs remains uniform.

Figure 6 shows the heat flux distributions of GNPs for five shapes. Owing to the high temperature on the upper surface, the value of heat flux is negative. It is clear that the absolute values of heat flux in the loading direction decrease gradually from the center to the edge. Comparing five shapes of GNPs, it can be found that the heat fluxes of elliptic and rectangular GNPs are higher than those of the others. Due to the higher thermal conductivity of GNPs, GNPs will offer more thermal conducting paths and most of the heat flow is transferred from GNPs.

Figure 7 shows the heat flux distributions of Al matrix for five GNPs shapes. Compared with Fig. 6, it is obvious that the heat flux of the matrix is significantly lower than that of GNPs. The heat flux varies from  $2.248 \times 10^5$  to  $1.060 \times 10^6 \text{ mW/mm}^2$ , which is almost one order of magnitude lower than that of GNPs. Besides, the existence of GNPs leads to the uneven heat flux distribution in the matrix, and the maximum absolute values of heat flux occur at the interface between GNPs and matrix along the loading direction, which indicates that a large amount of heat flux is gathered here. If the heat flux distributions of GNPs and matrix are superimposed, the formation of heat flux channel is obvious (indicated by the arrows in Fig. 7a, b, d). In the same way, it can be found the heat fluxes of the matrix filled with elliptical and rectangular GNPs are higher than those of the others. This can be explained that the longer

the effective length along the loading direction is, the closer the interfaces are, and the easier the continuous heat flow channel is formed.

The average heat fluxes of all nodes in the GNP/Al composites were calculated according to the simulation results, and the effective thermal conductivity of the composites with five GNP shapes is shown in the Fig. 8. It is obvious that the thermal conductivities of GNP/Al composites for all GNPs shapes are significantly higher than that of aluminum. The thermal conductivity with elliptic GNPs is the highest, and that of square GNPs is the lowest. The highest and lowest thermal conductivities are 275 W/m K and 264 W/m K, which are 27% and 22% higher than that of aluminum matrix, respectively. The reason is that the maximum effective length of elliptical GNP in the heat transfer direction ( $x$  negative direction) is larger than other shapes, and then, the heat flow channel is more continuous.

### 3.2 Influence of Aspect Ratio

In order to analyze the influence of the aspect ratio (diameter/thickness) of GNPs on the thermal conductivity of the composites, circle GNPs with a thickness of 5 nm were selected. The volume fraction remains a constant, and five RVE models of GNP/Al composites were established by changing the GNP diameter, as shown in Fig. 9. The volume fraction of GNPs is 0.25%, and the aspect ratios of GNPs are 20, 26, 40, 80 and 160, respectively.

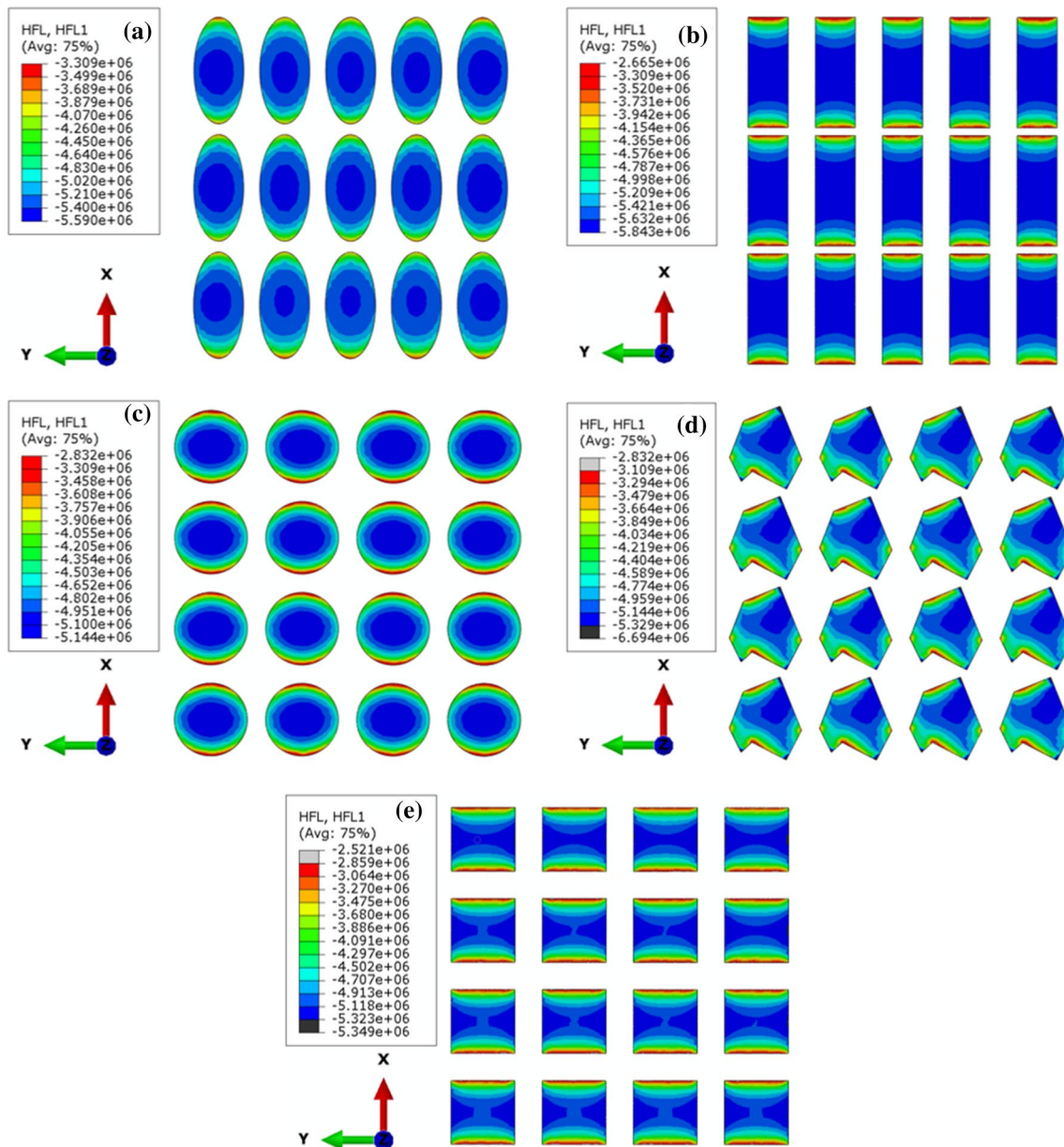


**Fig. 6** Heat flux of GNPs: **a** ellipse, **b** rectangle, **c** circle, **d** polygon, **e** square

Figure 10 shows a cross-sectional view of the heat fluxes of GNP/Al composites for five aspect ratios of GNPs. In order to compare the influence of GNPs aspect ratio on the thermal conductivity of GNP/Al composites, the same heat flux range is selected. From the figure, it can be seen that with the increase in aspect ratio, the maximum absolute value of heat flux of GNPs increases gradually, and the maximum absolute value region increases also.

In addition, the thermal conductivity of GNP/Al composites with different aspect ratios of GNPs is plotted in Fig. 11. It is obvious that with the increase in aspect ratio,

the thermal conductivity of GNP/Al composites increased rapidly at first, and when aspect ratio was larger than 80, the predicted average thermal conductivity tended to be unchanged. This is also consistent with the results reported by Min et al. [34] and Sebastien et al. [8] when they investigated the thermal conductivity of GNP/epoxy composites. The results of Sebastien et al. [8] showed that the hexagonal boron nitride sheets with a larger aspect ratio could enhance the oriented thermal conductivity of polymer composites dramatically.

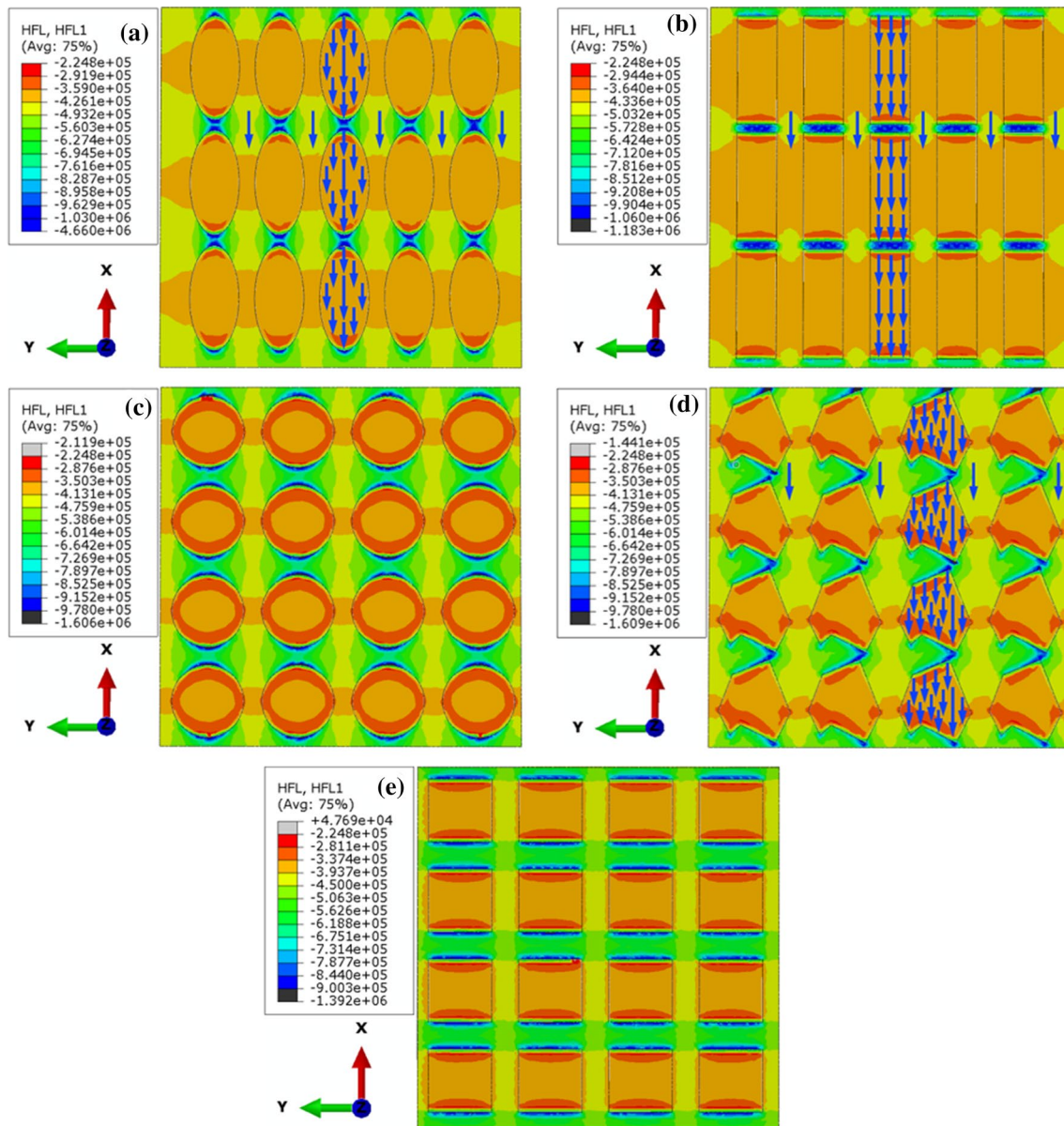


Fig. 7 Heat flux of matrix with GNP shapes of **a** ellipse, **b** rectangle, **c** circle, **d** polygon, **e** square

### 3.3 Influence of Geometric Configuration

Besides shape and aspect ratio of GNPs, the influence of configuration of GNPs was investigated. In the same way, circular GNPs with a thickness of 5 nm and aspect ratio of 40 were selected. The RVEs with five configurations were established, namely layered, evenly oriented, agglomerated, networked and randomly arranged, and the establishment of each configuration needed more GNPs than before. Therefore, the volume fraction of GNPs in this part was 1%, as shown in Fig. 12.

Figure 13 shows the heat flux distributions of GNPs for five configurations. It can be seen that the heat flux absolute

values of most GNPs with layered and evenly oriented configurations are high (see Fig. 13a, b). For the networked GNPs, the heat flux absolute value of GNPs arranged in the loading direction is high (see Fig. 13d). However, only a few GNPs have the high heat flux for agglomerated and randomly arranged configurations (see Fig. 13c, e). The reason is that there is a certain angle between the alignment direction of some GNPs and the loading direction for the two configurations, which greatly reduces the heat flux of GNPs. This further indicates that the position and orientation of GNPs have a great influence on the thermal conductivity of GNP/Al composites. Therefore, in order to efficiently utilize

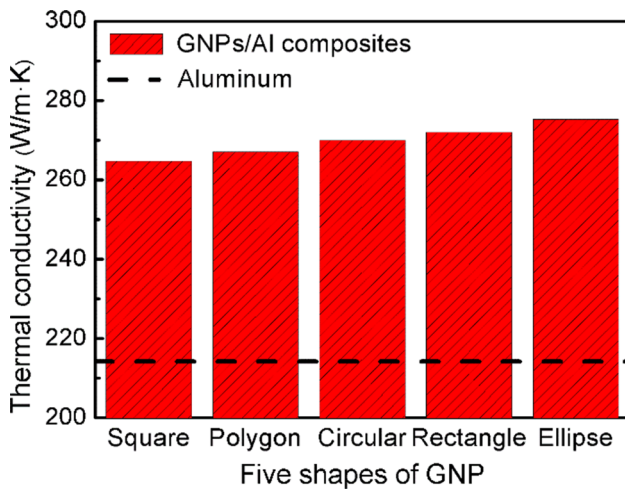


**Fig. 8** Thermal conductivity of GNP/Al composites with different shapes of GNPs

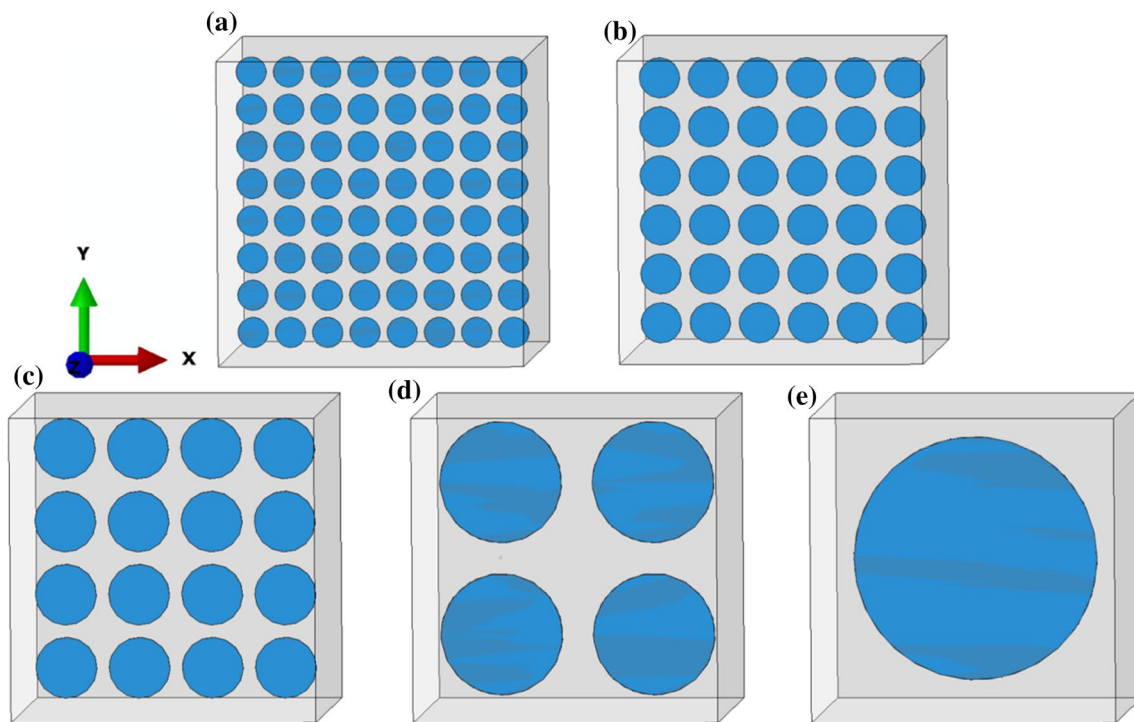
the superior thermal properties of GNPs, GNPs should be well dispersed and aligned along the loading direction.

Figure 14 shows the heat flux distributions of Al matrix for five GNP configurations. Similarly, the heat flux of the matrix is quite irregular, and the maximum absolute value of heat flux also occurs at the interface between GNPs and matrix along the loading direction. In addition, it is obvious that the configuration of GNPs has a great influence on the heat flux distribution in the matrix. In the same way, if

the heat flow distributions of GNPs and matrix are superimposed, it is easy to see that many heat flow channels can be formed on the matrix when GNPs are layered (indicated by the arrows in Fig. 14a). When GNPs configuration is agglomerated, only one heat channel can be formed (see Fig. 14c). For the other three cases, the interface is far away from each other; therefore, few effective heat flow channels can be formed (see Fig. 14b, d, e).

To further explore the change of heat flux caused by alignment direction, GNPs with different alignment directions were selected from five configurations. As shown in Fig. 15, five different angles between the loading direction ( $x$  positive direction) and GNPs were selected, namely  $0^\circ$ ,  $24^\circ$ ,  $43^\circ$ ,  $60^\circ$ ,  $89^\circ$ . The path ‘point 1–point 5’ has been chosen, which includes GNP and the matrix positions close to and far from the GNPs.

Figure 16 shows the heat flux of each point on the path at different alignment angles. It can be seen that the heat flux values of point 1 and point 5 are the same, which are far from the GNPs. The heat flux values of point 2 and point 4 are the same, which are close to the GNPs. The heat flux values of points 2 and 4 are lower than that of points 1 and 5. In other words, the closer the matrix is to the GNP, the smaller the heat flux is. The reason is that due to the high thermal conductivity of the GNP, most of the heat flux preferentially flows out of GNP, and then, the heat flux of the matrix close to GNP is lower. Meanwhile, it can be found that the alignment direction of GNP has little effect on the



**Fig. 9** RVE with aspect ratios of **a** 20, **b** 26, **c** 40, **d** 80, **e** 160

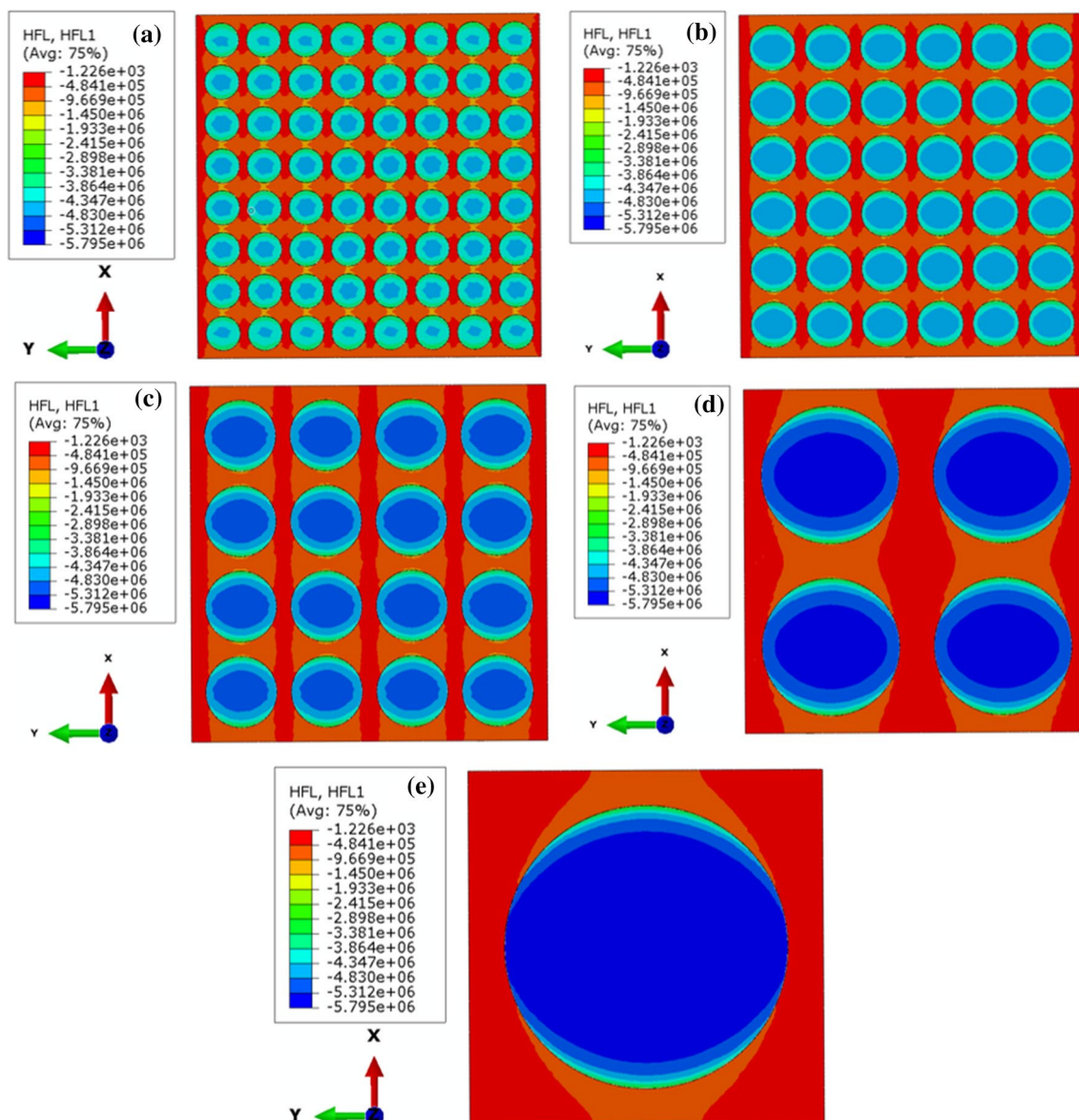


Fig. 10 Heat flux distributions of GNP/Al composites with GNP aspect ratios of a) 20, b) 26, c) 40, d) 80, e) 160

heat flux values of the matrix. As expected, the alignment angle has a significant influence on the heat flux of GNP (point 3). Figure 17 shows the variation of GNP heat flux with the alignment angle, and the dotted line represents the linear fitting curve, which can be expressed as:

$$q_G = (-0.0486\alpha + 5.40718) \times 10^6, \quad 0 \leq \alpha \leq 90 \quad (6)$$

where  $q_G$  is the heat flux value of the GNP,  $\alpha$  is the alignment angle. It can be seen that with increasing the angle between the loading direction and the GNP, the heat flux value of GNP decreases linearly.

The effective thermal conductivities of GNP/Al composites for five configurations have been calculated by Eq. (2), as shown in Fig. 18. It can be seen that the thermal conductivity of the GNP/Al composites with the layered configuration is the highest, followed by the evenly oriented and agglomerated, and the randomly arranged is the lowest. The reason is that the randomly arranged GNPs in the matrix increase unneeded heat diffusion in other directions, resulting in reduced thermal diffusion in one specific direction. Therefore, the more heat flow channels formed in the GNP/Al composite, the higher the effective thermal conductivity. This is also consistent with the experimental results [35, 36].

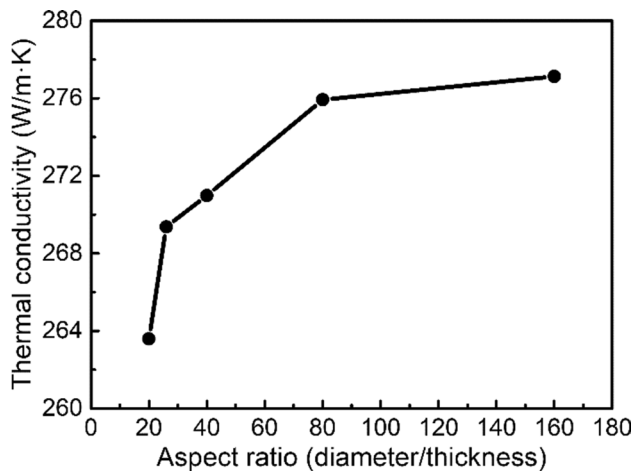


**Fig. 11** Thermal conductivity of GNP/Al composites with different aspect ratios of GNPs

### 3.4 Influence of Volume Fraction

It is well known that the thermal conductivity of GNP/Al composites can be effectively improved by increasing the volume fraction of GNPs [37]. Therefore, in order to obtain a new high-performance GNP/Al composite and

help researchers optimize practical manufacturing process in future, it is necessary to investigate the influence of GNPs volume fraction on the thermal conductivity.

The above results shown that GNP/Al composites with layered structure have the highest thermal conductivity, and the thermal conductivity of GNP/Al composites with layered configuration has been calculated for different volume fractions of GNP. Figure 19 shows the variation of the thermal conductivity of GNP/Al composites as a function of GNPs volume fraction change. As expected, the thermal conductivity increases almost linearly with the increase in the volume fraction of GNPs. When the volume fraction is 1.54%, the thermal conductivity of GNPs/Al composite can reach 400 W/m K, which increased about 84% compared with that of Al. This thermal conductivity is close to that of copper, while the density is only 1/6 of that of copper. Owing to the very high thermal conductivity of GNPs, the thermal conductivity of GNP/Al composites with layered configuration can be improved remarkably even at a low GNPs volume fraction.

To validate the numerical model of GNP/Al composites, the thermal conductivity of GNP/Al composites with random configuration, calculated theoretically and experimental data from different literatures [38, 39] are also shown in Fig. 19. It is obvious that the thermal conductivity of the composites with layered configuration is much higher

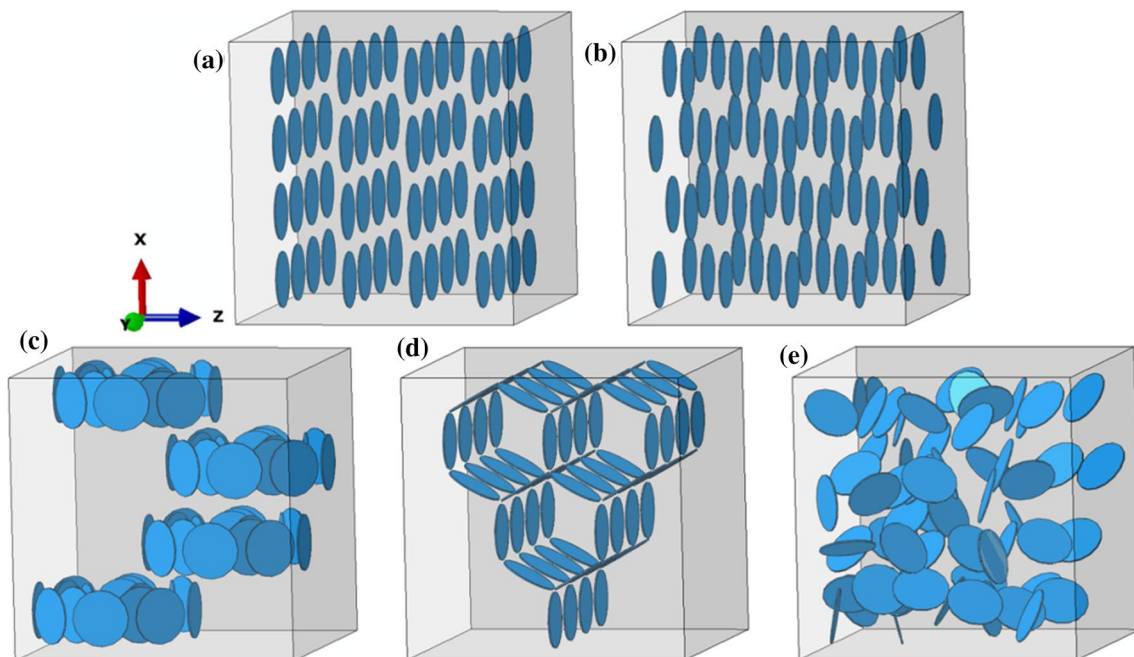


**Fig. 12** Schematics of RVE with GNPs configurations of **a** layered, **b** evenly oriented, **c** agglomerated, **d** networked, **e** randomly arranged

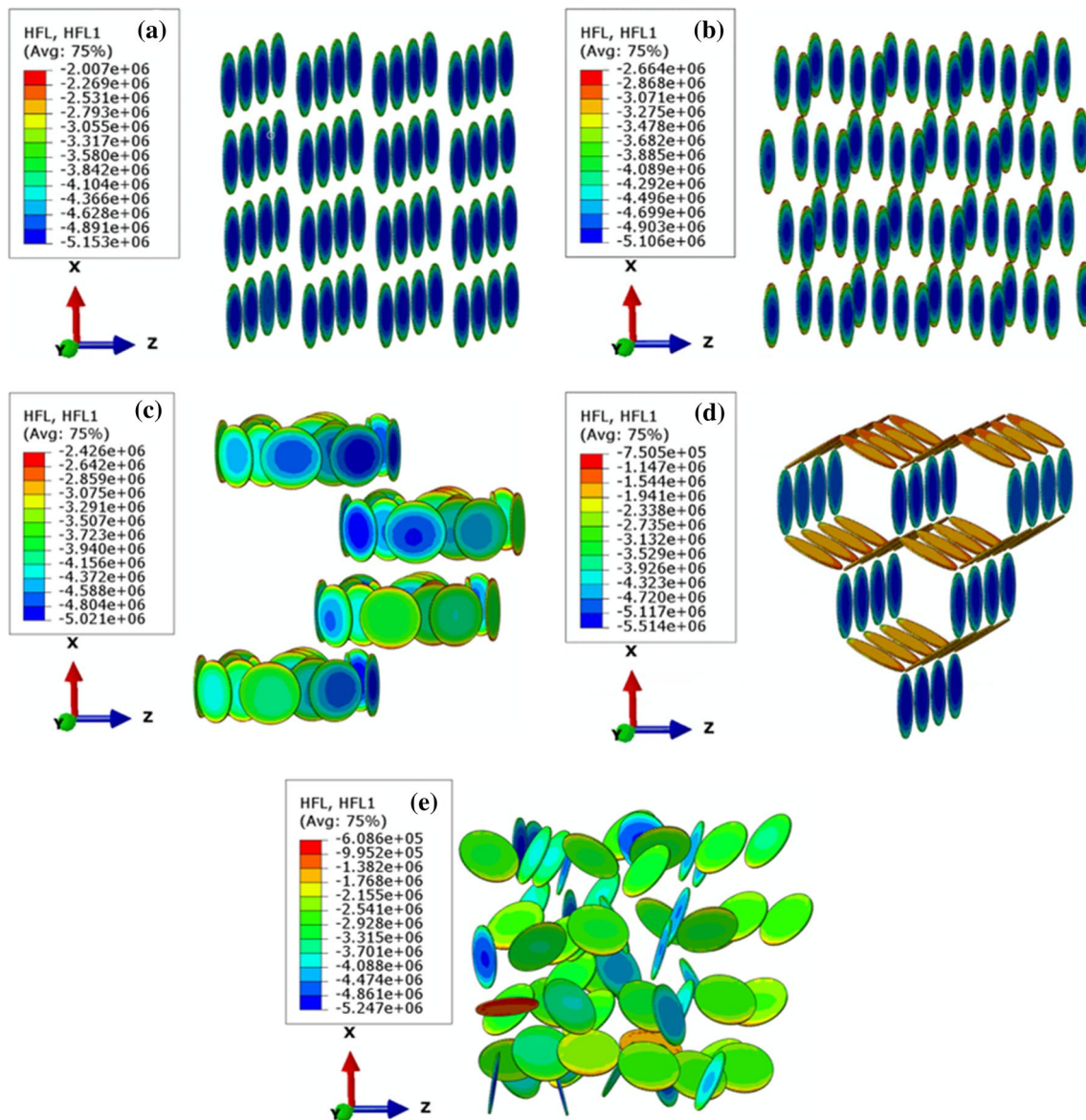


**Fig. 13** Heat flux of GNPs with different configurations: **a** layered, **b** evenly oriented, **c** agglomerated, **d** networked, **e** randomly arranged

than those of the calculated theoretically and experimental. However, the thermal conductivity of GNP/Al composites with random configuration is on a similar level with calculated theoretically and experimental values. The reason is that it is difficult to prepare the GNP/Al composites with ideal layered configuration in the experiment. On the other hand, the ROM model is based on the random distribution of reinforcement, without considering the anisotropy and

configuration of GNPs. Moreover, the thermal conductivity obtained from experiment has been improved at low GNPs volume fraction, while has little variation with the increasing of GNPs volume fraction. This could be attributed to the GNPs aggregation at high volume fraction. Therefore, comparing with the theoretical calculation, the FEM can consider the configuration, distribution and aggregation of GNPs in the matrix and predict the thermal conductivity of GNP/Al composites more accurate.

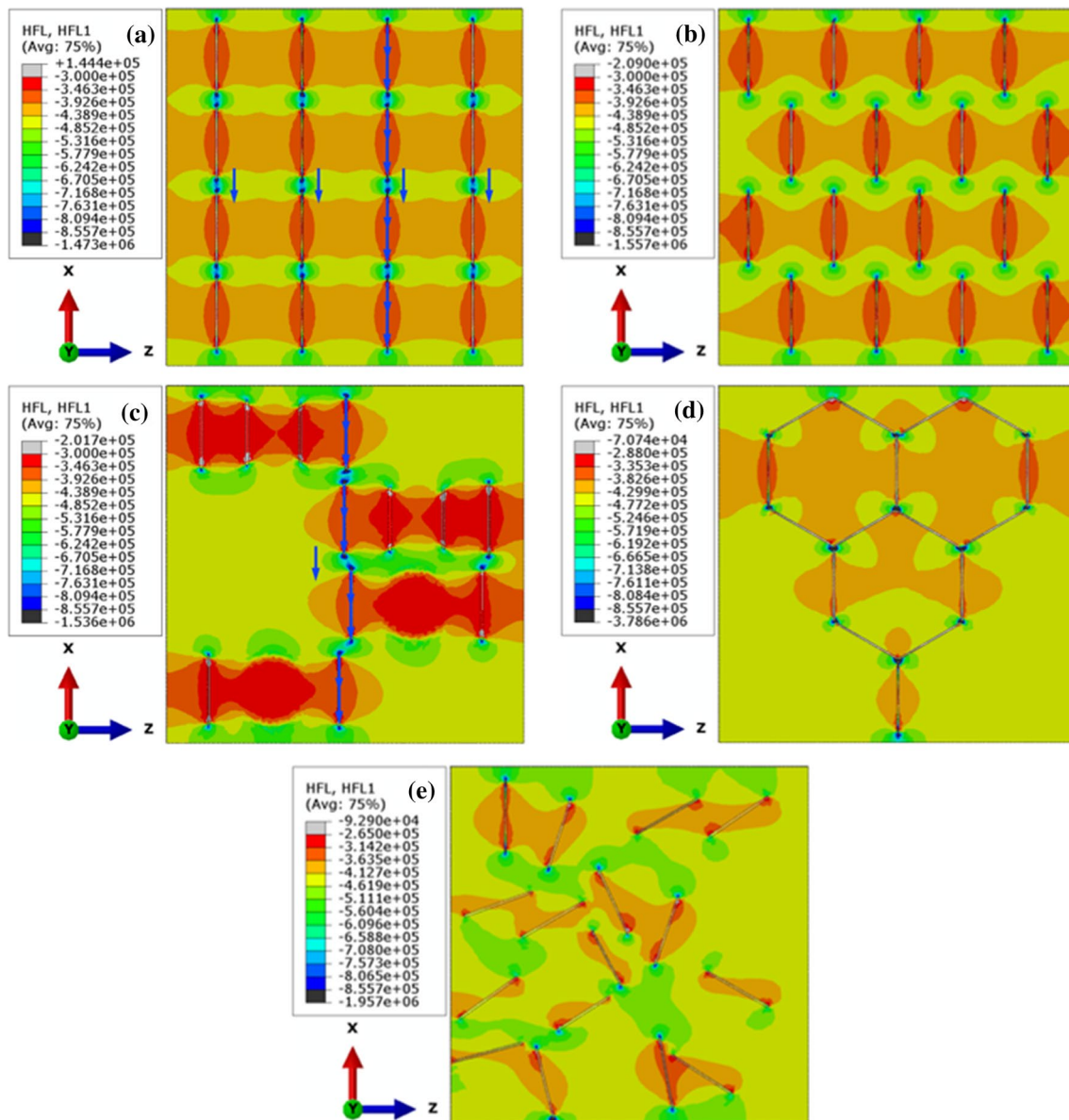


**Fig. 14** Heat flux of matrix with different configurations of GNPs: **a** layered, **b** evenly oriented, **c** agglomerated, **d** networked, **e** randomly arranged

## 4 Conclusions

1. The shape of GNPs has a little influence on the thermal conductivity of GNP/Al composites. Due to the different effective lengths of GNPs along the loading direction, the thermal conductivity with elliptic GNPs is the highest, and that of square GNPs is the lowest.
2. With the increase in aspect ratio, the thermal conductivity of GNP/Al composites increased rapidly at first, and when aspect ratio was larger than 80, the predicted average thermal conductivity tended to be unchanged.
3. The configuration of GNPs has a great influence on the effective thermal conductivities of GNP/Al composites. The thermal conductivity of the GNP/Al composites with the layered configuration is the highest, followed by the evenly oriented and agglomerated, and the randomly arranged is the lowest.
4. The thermal conductivity increases almost linearly with the increase in the volume fraction of GNPs. In the ideal condition, when the volume fraction of GNPs is 1.54%, the thermal conductivity of GNP/Al composites with layered configuration can reach 400 W/m K, which increased about 84% compared with that of Al.

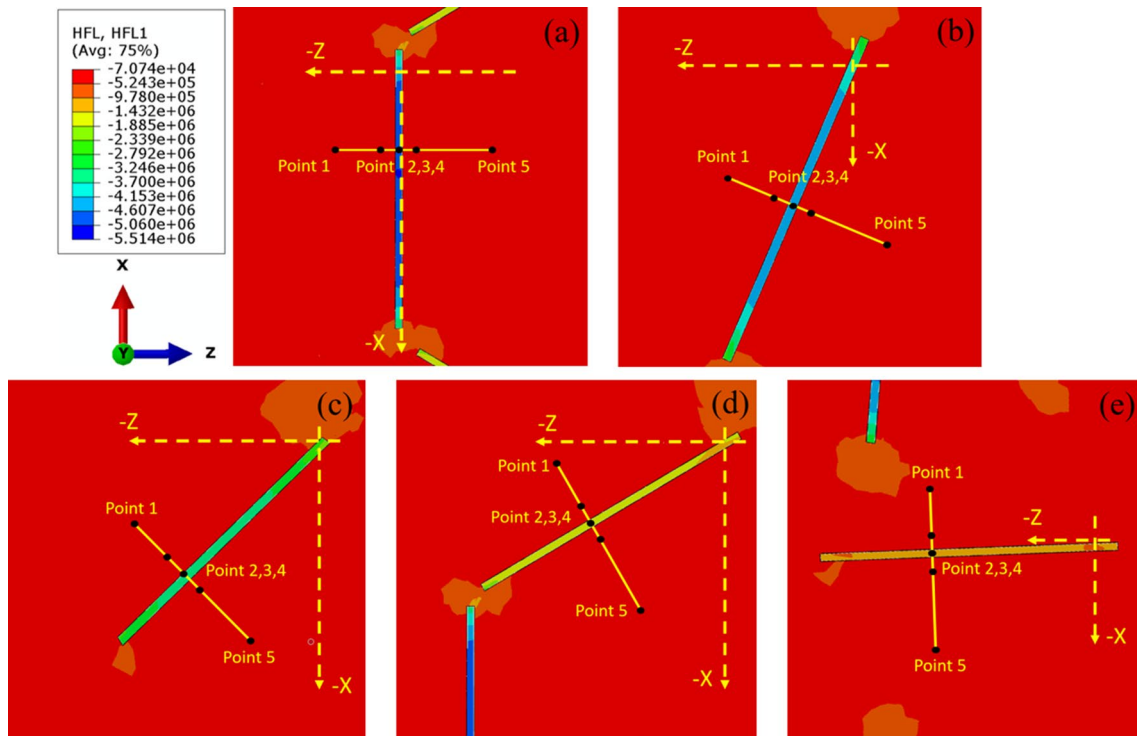


Fig. 15 Paths with different alignment angles of GNPs: a 0°, b 24°, c 43°, d 60°, e 89°

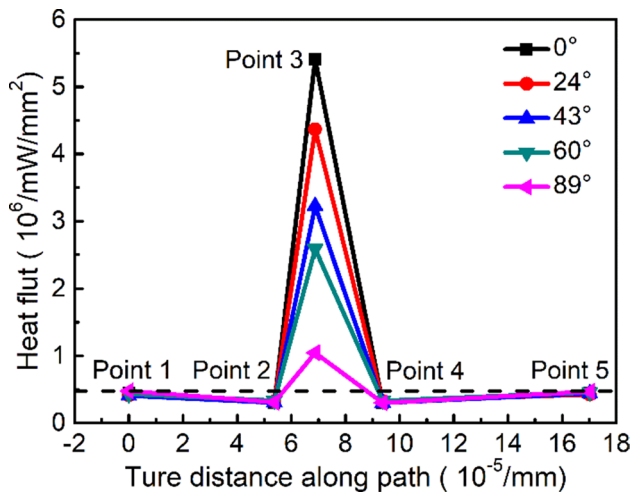


Fig. 16 Variation of heat flut along the path at different alignment angles of GNP

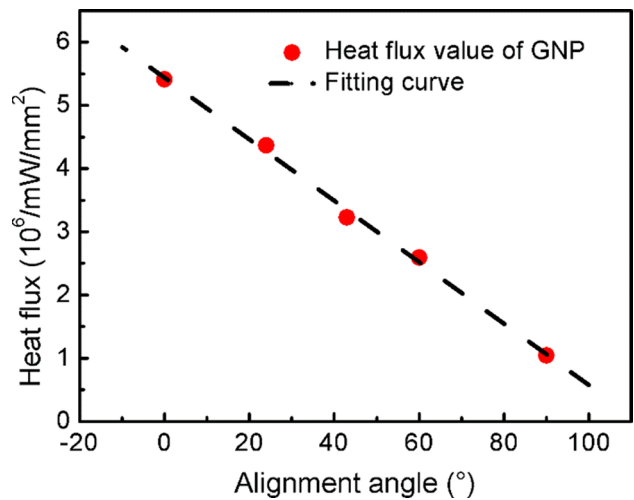
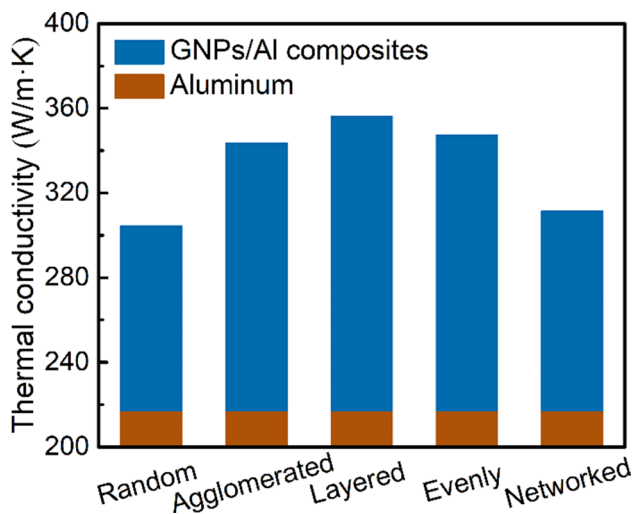
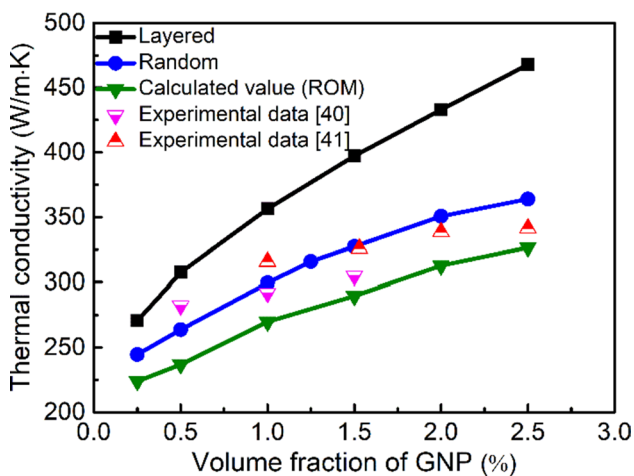


Fig. 17 Heat flux of GNP at different alignment angles



**Fig. 18** Thermal conductivity of GNP/Al composites with five GNP configurations



**Fig. 19** Thermal conductivity of GNP/Al composites for different GNP volume fractions

**Acknowledgements** This work is financially supported by the Key Research Program of Frontier Sciences, CAS (No. QYZDJ-SSW-JSC015); the National Natural Science Foundation of China (Nos. 51931009, 51871214 and 51871215); the National Key R&D Program of China (No. 2017YFB0703104).

## References

- [1] I. Tlili, T.A. Alkanhal, A.A. Barzinjy, R.N. Dara, A. Shafee, Z.X. Li, *J. Mol. Liq.* **294**, 111564 (2019)
- [2] A.A. Balandin, S. Ghosh, W.Z. Bao, I. Calizo, D. Teweldebrhan, F. Miao, C.N. Lau, *Nano Lett.* **8**, 902 (2008)
- [3] D.V. Thanh, N.V. Thien, B.H. Thang, N.V. Chuc, N.M. Hong, B.T. Trang, T.D. Lam, D.T.T. Huyen, P.N. Hong, P.N. Minh, *J. Electron. Mater.* **45**, 2522 (2016)
- [4] A. Bhadauria, L.K. Singh, T. Laha, *Mater. Sci. Eng. A* **749**, 14 (2019)
- [5] X.Q. Han, L.Z. Yang, N.Q. Zhao, C.N. He, *Acta Metall. Sin. Engl. Lett.* **34**, 111 (2021)

- [6] S.Y. Guo, X. Zhang, C.S. Shi, E.Z. Liu, C.N. He, F. He, N.Q. Zhao, *Powder Technol.* **362**, 126 (2020)
- [7] A. Saboori, M. Pavese, C. Badini, P. Fino, *Acta Metall. Sin. Engl. Lett.* **31**, 148 (2018)
- [8] S. Depaifve, S. Hermans, D. Ruch, A. Laachachi, *Thermochim. Acta* **691**, 178712 (2020)
- [9] W.S. Yang, G.Q. Chen, J. Qiao, S.F. Liu, R. Xiao, R.H. Dong, M. Hussain, G.H. Wu, *Mater. Sci. Eng. A* **700**, 351 (2017)
- [10] G. Li, B.W. Xiong, *J. Alloys Compd.* **697**, 31 (2017)
- [11] A. Bisht, M. Srivastava, R.M. Kumar, I. Lahiri, D. Lahiri, *Mater. Sci. Eng. A* **695**, 20 (2017)
- [12] B.Y. Ju, W.S. Yang, P.Z. Shao, M. Hussain, Q. Zhang, Z.Y. Xiu, X.W. Hou, J. Qiao, G.H. Wu, *Carbon* **162**, 346 (2020)
- [13] C.H. Jeon, Y.H. Jeong, J.J. Seo, H.N. Tien, S.T. Hong, Y.J. Yum, S.H. Hur, K.J. Lee, *Int. J. Precis. Eng. Manuf.* **15**, 1235 (2014)
- [14] A. Saboori, M. Pavese, C. Badini, P. Fino, *Acta Metall. Sin. Engl. Lett.* **30**, 675 (2017)
- [15] S. Polat, Y. Sun, E. Çevik, H. Colijn, *Diam. Relat. Mater.* **98**, 107457 (2019)
- [16] C.Y. Wang, Y.S. Su, Q.B. Ouyang, D. Zhang, *Diam. Relat. Mater.* **108**, 107929 (2020)
- [17] W. Evans, R. Prasher, J. Fish, P. Meakin, P. Phelan, P. Keblinski, *Int. J. Heat Mass Transf.* **51**, 1431 (2008)
- [18] W.K. Xiao, X. Zhai, P.F. Ma, T.T. Fan, X.T. Li, *Res. Phys.* **9**, 673 (2018)
- [19] Y.F. Zhang, Y.H. Zhao, S.L. Bai, X.W. Yuan, *Compos. B Eng.* **106**, 324 (2016)
- [20] Z.W. Xu, S.H. He, J.J. Zhang, S.J. Huang, A.F. Chen, X.L. Fu, P. Zhang, *Compos. Sci. Technol.* **183**, 107826 (2019)
- [21] M. Inagaki, Y. Kaburagi, Y. Hishiyama, *Adv. Eng. Mater.* **16**, 494 (2014)
- [22] S. Kumar, R.S. Bhoopal, P.K. Sharma, R.S. Beniwal, R. Singh, *Open. J. Compos. Mater.* **1**, 10 (2011)
- [23] A.A. Balandin, *Nat. Mater.* **10**, 569 (2011)
- [24] I.E. Monje, E. Louis, J.M. Molina, *J. Mater. Sci.* **51**, 8027 (2016)
- [25] Y.S. Su, Z. Li, Y. Yu, L. Zhao, Z.Q. Li, Q. Guo, D.B. Xiong, D. Zhang, *Sci. China Mater.* **61**, 112 (2018)
- [26] G. Dai, L. Mishnaevsky, *Compos. Sci. Technol.* **91**, 71 (2014)
- [27] P.L. Bian, S. Schmauder, H. Qing, *Compos. Struct.* **245**, 112337 (2020)
- [28] J.J. Chen, J.C. Han, *Results Phys.* **15**, 102803 (2019)
- [29] B.Z. Gao, J.Z. Xu, J.J. Peng, F.Y. Kang, H.D. Du, J. Li, S.W. Chiang, C.J. Xu, N. Hu, X.S. Ning, *Thermochim. Acta* **614**, 1 (2015)
- [30] W.L. Yang, J.Q. Sang, L.P. Zhou, K. Peng, J.J. Zhu, D.Y. Li, *Diam. Relat. Mater.* **81**, 127 (2018)
- [31] Z.F. Zhao, H. Chen, H.M. Xiang, F.Z. Dai, X.H. Wang, Z.J. Peng, Y.C. Zhou, *J. Mater. Sci. Technol.* **35**, 2892 (2019)
- [32] B.J. Yan, L. Cheng, B.Q. Li, P.C. Liu, X.W. Wang, R. Gao, Z.L. Yang, S.H. Xu, X.D. Ding, P.C. Zhang, *Mater. Des.* **189**, 108483 (2020)
- [33] Y.Y. Sun, L.Y. Zhou, Y. Han, L. Cui, L. Chen, *Int. J. Heat Mass Transf.* **160**, 120157 (2020)
- [34] C. Min, D.M. Yu, J.Y. Cao, G.L. Wang, L.H. Feng, *Carbon* **55**, 116 (2013)
- [35] C.P. Feng, S.S. Wan, W.C. Wu, L. Bai, R.Y. Bao, Z.Y. Liu, M.B. Yang, J. Chen, W. Yang, *Compos. Sci. Technol.* **167**, 456 (2018)
- [36] N. Song, D.J. Jiao, P. Ding, S.Q. Cui, S.F. Tang, L.Y. Shi, *J. Mater. Chem. C* **4**, 305 (2016)
- [37] B. Zhou, W. Luo, J.Q. Yang, X.B. Duan, Y.W. Wen, H.M. Zhou, R. Chen, B. Shan, *Compos. Part A Appl. Sci. Manuf.* **90**, 410 (2016)
- [38] J.K. Chen, I.S. Huang, *Compos. Part B Eng.* **44**, 698 (2013)
- [39] W.J. Li, Y. Liu, G.H. Wu, *Carbon* **95**, 545 (2015)